*Appl. Math. Mech. -Engl. Ed.*, **41**(9), 1417–1430 (2020)

**APPLIED MATHEMATICS AND MECHANICS (ENGLISH EDITION)**

https://doi.org/10.1007/s10483-020-2643-7

# Thermal analysis in swirl motion of Maxwell nanofluid over a rotating circular cylinder*

A. AHMED[1], M. KHAN[1], J. AHMED[1,2,†]

1. Department of Mathematics, Quaid-i-Azam University, Islamabad 44000, Pakistan;
2. Department of Basic Sciences, University of Engineering and Technology, Taxila 47050, Pakistan

(Received Feb. 24, 2020 / Revised May 23, 2020)

**Abstract** In this paper, the mechanism of thermal energy transport in swirling flow of the Maxwell nanofluid induced by a stretchable rotating cylinder is studied. The rotation of the cylinder is kept constant in order to avoid the induced axially secondary flow. Further, the novel features of heat generation/absorption, thermal radiation, and Joule heating are studied to control the rate of heat transfer. The effects of Brownian and thermophoretic forces exerted by the Maxwell nanofluid to the transport of thermal energy are investigated by utilizing an effective model for the nanofluid proposed by Buongiorno. The whole physical problem of fluid flow and thermal energy transport is modelled in the form of partial differential equations (PDEs) and transformed into nonlinear ordinary differential equations (ODEs) with the help of the suitable flow ansatz. Numerically acquired results through the technique bvp4c are reported graphically with physical explanation. Graphical analysis reveals that there is higher transport of heat energy in the Maxwell nanoliquid for a constant wall temperature (CWT) as compared with the prescribed surface temperature (PST). Both thermophoretic and Brownian forces enhance the thermal energy transport in the flowing Maxwell nanofluid. Moreover, the temperature distribution increases with increasing values of the radiation parameter and the Eckert number. It is also noted that an increase in Reynolds number reduces the penetration depth, and as a result the flow and transport of energy occur only near the surface of the cylinder.

**Key words** Maxwell nanofluid, rotating cylinder, heat source/sink, Joule heating, convective condition, numerical solution

**Chinese Library Classification** O361
**2010 Mathematics Subject Classification** 76R05, 76E07, 76A05

## Nomenclature

| | | | |
|---|---|---|---|
| $\alpha$, | stretching rate ($\mathrm{T}^{-1}$); | $C_{\mathrm{w}}$, | wall concentration; |
| $B$, | magnetic field; | $Re$, | Reynolds number; |
| $B_0$, | strength of magnetic field ($\mathrm{N\cdot m\cdot A}^{-1}$); | $Sh$, | Sherwood number; |
| $C$, | concentration in fluid; | $T$, | temperature of fluid (K); |

* Citation: AHMED, A., KHAN, M., and AHMED, J. Thermal analysis in swirl motion of Maxwell nanofluid over a rotating circular cylinder. *Applied Mathematics and Mechanics* (*English Edition*), **41**(9), 1417–1430 (2020) https://doi.org/10.1007/s10483-020-2643-7

† Corresponding author, E-mail: j.ahmed@math.qau.edu.pk

$T_{\mathrm{w}}$, wall temperature (K);
$T_{\infty}$, ambient fluid temperature (K);
$C_{\infty}$, ambient concentration;
$c_p$, specific heat capacity ($\mathrm{J{\cdot}K^{-1}{\cdot}kg^{-1}}$);
$D_{\mathrm{B}}$, mass diffusivity ($\mathrm{m^2{\cdot}s^{-1}}$);
$D_{\mathrm{T}}$, thermophoresis coefficient ($\mathrm{m^2{\cdot}s^{-1}}$);
$E$, rotational velocity ($\mathrm{m{\cdot}s^{-1}}$);
$Ec_1$, Eckert number due to surface stretching;
$Ec_2$, Eckert number due to surface rotation;
$f'$, dimensionless axial velocity;
$\frac{f(\eta)}{\eta^{1/2}}$, dimensionless radial velocity;
$g$, dimensionless azimuthal velocity;
$h_{\mathrm{t}}$, heat transfer coefficient ($\mathrm{W{\cdot}m^{-2}{\cdot}K^{-1}}$);
$Le$, Lewis number;
$M$, magnetic number;
$N_{\mathrm{t}}$, thermophoretic parameter;
$N_{\mathrm{b}}$, Brownian diffusion parameter;
$Nu$, Nusselt number;
$Pr$, Prandtl number;
$Q_0$, heat source/sink coefficient;
$r$, radial coordinate;
$R_{\mathrm{d}}$, radiation parameter;
$u$, axial velocity component;
$u_{\mathrm{s}}$, surface stretching velocity ($\mathrm{m{\cdot}s^{-1}}$);
$V$, velocity field;
$v$, azimuthal velocity component;
$v_{\mathrm{r}}$, surface rotation velocity ($\mathrm{m{\cdot}s^{-1}}$);
$w$, radial velocity components ($\mathrm{m{\cdot}s^{-1}}$);
$z$, axial coordinate;
$\varphi$, azimuthal coordinate;
$\lambda_1$, fluid relaxation time ($\mathrm{T^{-1}}$);
$\nu$, kinematic velocity ($\mathrm{m^2{\cdot}s^{-1}}$);
$\sigma$, electric conductivity of fluid ($\mathrm{S{\cdot}m^{-1}}$);
$\rho$, density of fluid ($\mathrm{kg{\cdot}m^{-3}}$);
$\eta$, dimensionless variable;
$\alpha_1$, thermal diffusivity of fluid ($\mathrm{m^2{\cdot}s^{-1}}$);
$\mu$, dynamic viscosity ($\mathrm{kg{\cdot}m^{-1}{\cdot}s^{-1}}$);
$\theta$, dimensionless temperature;
$\beta_1$, Maxwell parameter;
$\gamma_1$, Biot number;
$\tau$, heat capacity ratio;
$\delta$, source/sink parameter.

## 1 Introduction

In this era of fast-growing technology, the subject of non-Newtonian fluid flow has fascinated the scientists due to its numerous applications in the fields of engineering, such as glass blowing, adhesive tapes processing, and coating application, which often require the flow of non-Newtonian fluids over a rigid surface. Although the flow behavior of Newtonian fluids is described by the simple linear relationship between shear stress and shear rate, non-Newtonian fluids have the complex rheological properties depending on their viscosity behavior as a function of shear rate, stress, deformation history, etc. Each non-Newtonian fluid has its own characteristics and thus there is no single mathematical relation which can explain the flow behavior of all non-linear fluids. Therefore, scientists classified non-Newtonian fluids into three main types: (i) differential type, (ii) integral type, and (iii) rate type by defining the mathematical model for each specific non-Newtonian fluid. Flows of non-Newtonian fluids in various geometries with various physical assumptions were reported in Refs. [1]–[4]. The Phan-Thien-Tanner model was employed by Dhinakaran et al.[5] to investigate the steady flow of viscoelastic fluid between parallel plates under the effect of electro-osmotic forces. Prasad et al.[6] studied the magnetohydrodynamic (MHD) flow of viscoelastic fluid with variable viscosity and heat transport over a stretching sheet. Their analysis revealed that higher values of magnetic parameter decrease the surface temperature gradient and skin friction. Malaspinas et al.[7] utilized the lattice Boltzmann method to simulate linear and non-linear viscoelastic fluids. Siddiqa et al.[8] numerically examined the free convection flow of non-Newtonian fluid over a vertical surface. In the recent studies of non-Newtonian fluids, the non-axisymmetric Homann flow problem for the viscoelastic fluid over a fixed plate was investigated numerically by Mahapatra and Sidui[9]. Dimensionless velocities and displacement thickness were analyzed for different values of viscoelastic parameter in their study.

In non-linear fluids, viscoelastic fluids exhibit both the elastic and viscous effects, and the stress-strain relationship depends on time for these fluids. Two major phenomena are observed in viscoelastic fluids: one is stress relaxation and the other is creep. Thus, researchers have proposed two mathematical models for these types of fluids which are the Maxwell model and the Kelvin Voigt model. The Maxwell fluid model is the simplest model for linear viscoelastic

type material to describe the phenomenon of stress relaxation. On the other hand, the Kelvin Voigt model can predict the creep phenomenon but this model is poor for stress relaxation. Most materials found in industries are viscoelastic fluids under stress relation behavior, such as process of manufacturing of plastic, paints, polymers, and rubber sheets. On the other hand, there are some limitations of the present Maxwell fluid model. This model can only predict the stress relaxation phenomenon in the viscoelastic fluid, and the model is poor for the creep phenomenon. Moreover, the shear thinning and shear thickening features cannot be described by this model. Attention has been paid by researchers to study the rheology of Maxwell fluid flow subject to various physical effects. Tan et al.[10] reported the investigation on an unsteady flow of Maxwell fluid between parallel plates. The Laplace and Fourier transforms were used for the solution of the problem. Nadeem et al.[11] numerically studied the flow of Maxwell fluid induced by a stretching sheet under the effect of a magnetic field. They revealed that higher values of the relaxation time parameter decline the flow velocity and enhance the temperature distribution. Falkner-Skan flow of MHD Maxwell fluid was studied by Abbasbandy et al.[12]. In this study, both the analytical and numerical solutions were presented. In the recent investigations, Ahmed et al.[13] studied the swirling flow of Maxwell fluid between two coaxially rotating disks. Their results indicated that for a higher Reynolds number, the pressure field drops near the surface of lower disk. Rauf et al.[14] examined the multi-layer flows of an immiscible fractional Maxwell fluid. They obtained the analytical solution of the problem with the help of Laplace transform coupled with the Hankel and Weber transform of zero order. It was shown that the velocity decreases for higher values of the fractional parameter.

Heat transport in both types of fluids, linear and non-linear, plays a significant role in many engineering processes for both internal and external flow systems, e.g., cooling of electronic equipment, cooling of nuclear reactors, extrusion process, and energy conversion in nuclear reactors. Heat transport in the viscoelastic type fluid flow induced by rotating and stretching surfaces has a critical importance in plastic manufacturing because the quality of the final product greatly depends on it. Many studies were carried out by researchers in order to predict the heat transport in the flow due to stretching and rotating surfaces[15–19]. Analysis of thermal energy transport in mixed convection flow of viscous fluid over a nonlinear deforming surface under the effect of magnetic field was discussed by Turkyilmazoglu[20]. Heat transport in the stagnation point flow of Maxwell nanofluid over a rotating disk subject to heat generation/absorption was studied by Ahmed et al.[21]. The outcomes of their study revealed that the thermophoretic force enhances the thermal energy transport in the flow. Mehmood et al.[22] examined the convective heat transport mechanism in the viscous flow induced by the wavy rotating disk. Heat transport in the flow due to the rotating cylinder, confined with the non-Newtonian power-law fluid, was predicted by Thakur et al.[23]. They presented their results in the form of Nusselt number by using appropriate correlation.

Flow over rotating cylinders is significant in an extensive number of applications from shafts and axles to spinning projectiles. Recently, numerous researchers have studied the incompressible flow around a rotating circular cylinder using numerical, theoretical, and experimental methods. Many applications of this field can be found in aerodynamic problems as well as engineering structures. The boundary layer flows can be controlled through using rotational cylinders or other control methods such as Lorentz forces, blowing, suction, and surface roughness. In view of the above-studied rotating flows, it is noted that investigations deal with the investigation of thermal energy transport in the flow Maxwell nanofluid induced by stretching surfaces. Thus, the present work is proposed to analyze the rheology of three-dimensional (3D) boundary layer flow of Maxwell nanofluid with thermal energy transport induced by the rotating cylinder. The analysis of heat transport is carried out with the effect of Joule heating and heat generation/absorption in the flow of nanofluid. The surface temperature of the cylinder is considered as a constant and axially varying. Moreover, the convective heat transport at the surface of the cylinder is also considered. The physical problem is modelled in the form of par-

tial differential equations (PDEs) and transformed into a set of non-linear ordinary differential equations (ODEs) by using the appropriate flow similarities. The MATLAB scheme bvp4c is used for the numerical computations of the resulting ODEs. The acquired results are presented graphically with physical explanation.

## 2 Mathematical formulation

Consider an electrically conducting swirling flow of Maxwell nanofluid induced by a stretchable rotating cylinder with radius $R_1$ in the presence of a transverse magnetic field. The velocity field for flow is assumed as $V = (u, v, w)$, where $u$, $v$, and $w$ are velocity components along the $z$-, $\varphi$-, and $r$-axes, respectively, and $B = (0, 0, B_0)$ is the uniform magnetic field which is applied in the $r$-axis direction. We assume that the stretching velocity of the cylinder is directly proportional to axial distance, and the rotation of the cylinder is constant around its axis. Thermal analysis is investigated by considering the temperatures at the surface of the cylinder as $T(z, R_1) = T_{\mathrm{w}}$ (constant wall temperature (CWT)) and $T(z, R_1) = T_\infty + bz$ (prescribed surface temperature (PST)). The flow mechanism is presented in Fig. 1.

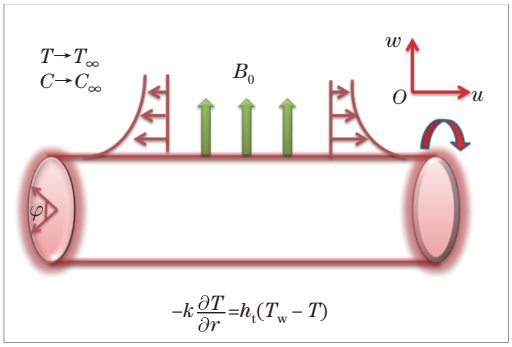


**Fig. 1** Schematic diagram for flow configuration (color online)

The extra stress tensor $S$ for the Maxwell fluid[24] is defined as

$$\left(1 + \lambda_1 \frac{\mathrm{D}}{\mathrm{D}t}\right) S = \mu A_1, \tag{1}$$

where $\lambda_1$ is the relaxation time, $\frac{\mathrm{D}}{\mathrm{D}t}$ signifies the upper convective derivative, $S$ is the extra stress tensor, $A_1 = \nabla V + (\nabla V)^{\mathrm{T}}$ signifies the first Rivlin-Ericksen tensor, and $\mu$ is the dynamic viscosity of the fluid. If $\lambda_1 = 0$ in the above equation, the case of Newtonian fluid can be recovered.

The basic transport equations for fluid flow, thermal, and solutal energy transport are found by conservation laws as

$$\nabla \cdot V = 0, \tag{2}$$

$$\rho \frac{\mathrm{d}V}{\mathrm{d}t} = -\nabla p + \nabla \cdot S + J_1 \times B, \tag{3}$$

$$\frac{\mathrm{d}T}{\mathrm{d}t} - \tau \left( D_{\mathrm{B}} \nabla C \cdot \nabla T + \frac{D_{\mathrm{T}}}{T_\infty} (\nabla T)^2 \right) = -\frac{1}{\rho c_p} \nabla \cdot q + \frac{J_1^2}{\sigma} + \frac{Q_0 (T - T_\infty)}{\rho c_p}, \tag{4}$$

$$\frac{\mathrm{d}C}{\mathrm{d}t} - \frac{D_{\mathrm{T}}}{T_\infty} \nabla^2 T = -\nabla \cdot J. \tag{5}$$

In the above equations, $\frac{\mathrm{d}}{\mathrm{d}t}$ is the material derivative, $\mu$ is the dynamic viscosity, $J_1$ is the current density, $\rho$ is the density of the fluid, $c_p$ is the heat capacity at constant pressure, $\tau$ is the effective heat capacity of nanoparticles to the base fluid, $D_{\mathrm{B}}$ is the Brownian diffusion

coefficient, $D_{\mathrm{T}}$ is the thermophoresis, and $Q_0$ is the heat generation source. Also, $T$ and $C$ are the temperature and concentration of the fluid, respectively, $T_\infty$ and $C_\infty$ are the free stream temperature and concentration, respectively, and $q$ and $J$ are heat and mass fluxes which are defined from classical Fourier's and Fick's laws, respectively.

Based on the assumptions of axisymmetric, steady, and incompressible, the governing boundary layer equations of the present flow and energy transport problem are obtained as

$$\frac{\partial u}{\partial z}+\frac{w}{r}+\frac{\partial w}{\partial r}=0, \tag{6}$$

$$\begin{aligned}&u\frac{\partial u}{\partial z}+w\frac{\partial u}{\partial r}+\lambda_1\Big(u^2\frac{\partial^2 u}{\partial z^2}+2uw\frac{\partial^2 u}{\partial r\partial z}+w^2\frac{\partial^2 u}{\partial r^2}\Big)\\ =&\nu\Big(\frac{\partial^2 u}{\partial r^2}+\frac{1}{r}\frac{\partial u}{\partial r}\Big)-\frac{\sigma B_0^2}{\rho}\Big(u+\lambda_1 w\frac{\partial u}{\partial r}\Big),\end{aligned} \tag{7}$$

$$\begin{aligned}&u\frac{\partial v}{\partial z}+w\frac{\partial v}{\partial r}+\frac{wv}{r}+\lambda_1\Big(u^2\frac{\partial^2 v}{\partial z^2}+2uw\frac{\partial^2 v}{\partial r\partial z}+w^2\frac{\partial^2 v}{\partial r^2}+\frac{2wv}{r}\frac{\partial w}{\partial r}+\frac{2uv}{r}\frac{\partial w}{\partial z}-\frac{2w^2v}{r^2}\Big)\\ =&\nu\Big(\frac{\partial^2 v}{\partial r^2}-\frac{v}{r^2}+\frac{1}{r}\frac{\partial v}{\partial r}\Big)-\frac{\sigma B_0^2}{\rho}\Big(v+\lambda_1 w\frac{\partial v}{\partial r}-\lambda_1\frac{wv}{r}\Big),\end{aligned} \tag{8}$$

$$\begin{aligned}u\frac{\partial T}{\partial z}+w\frac{\partial T}{\partial r}=&\alpha_1\Big(\frac{\partial^2 T}{\partial r^2}+\frac{1}{r}\frac{\partial T}{\partial r}\Big)+\tau\Big(D_{\mathrm{B}}\frac{\partial C}{\partial r}\frac{\partial T}{\partial r}+\frac{D_{\mathrm{T}}}{T_\infty}\Big(\frac{\partial T}{\partial r}\Big)^2\Big)\\ &-\frac{1}{\rho c_p}\frac{1}{r}\frac{\partial}{\partial r}(rq_{\mathrm{r}})+\frac{\sigma B_0^2}{\rho c_p}(u^2+v^2)+\frac{Q_0}{\rho c_p}(T-T_\infty),\end{aligned} \tag{9}$$

$$u\frac{\partial C}{\partial z}+w\frac{\partial C}{\partial r}=D_{\mathrm{B}}\Big(\frac{\partial^2 C}{\partial r^2}+\frac{1}{r}\frac{\partial C}{\partial r}\Big)+\frac{D_{\mathrm{T}}}{T_\infty}\Big(\frac{\partial^2 T}{\partial r^2}+\frac{1}{r}\frac{\partial T}{\partial r}\Big) \tag{10}$$

with the corresponding boundary conditions (BCs)

$$u_{\mathrm{s}}(z,r)=2az,\quad v_{\mathrm{s}}(z,r)=E,\quad w(z,r)=0,\quad -k\frac{\partial T}{\partial z}=h_{\mathrm{t}}\left(T_{\mathrm{w}}-T\right),\quad C=C_{\mathrm{w}}\ \text{ at }\ r=R_1, \tag{11}$$

$$u\to 0,\quad v\to 0,\quad T\to T_\infty,\quad C\to C_\infty\quad \text{as}\quad r\to\infty. \tag{12}$$

Here, $\nu$ is the kinematic viscosity, $\sigma$ is the electric conductivity of fluid, $\alpha_1$ is the thermal diffusivity, $B_0$ is the magnetic field strength, $a\ (>0)$ signifies the stretching strength of cylinder having dimension $T^{-1}$, $E$ is the torsional motion of cylinder with dimension as the same as the velocity, and $h_{\mathrm{t}}$ is the heat transfer coefficient. Moreover, $q_{\mathrm{r}}=\frac{-16\sigma^*}{3k^*}T_\infty^3\frac{\partial T}{\partial r}$ is the radiative heat flux, where $\sigma^*$ and $k^*$ are the Stefan-Boltzmann constant and mean absorption coefficient, respectively.

We introduce the following transformation group[25]:

$$\begin{cases}u=2azf'(\eta),\quad v=Eg(\eta),\quad w=-aR_1\dfrac{f(\eta)}{\eta^{1/2}},\\ \theta(\eta)=\dfrac{T-T_\infty}{T_{\mathrm{w}}-T_\infty}\quad\text{at}\quad\text{CWT},\quad \theta(\eta)=\dfrac{T-T_\infty}{bz}\quad\text{at}\quad\text{PST},\\ \phi(\eta)=\dfrac{C-C_\infty}{C_{\mathrm{w}}-C_\infty},\quad \eta=\dfrac{r^2}{R_1^2}.\end{cases} \tag{13}$$

After insertion of the above ansatz, Eq. (6) is satisfied automatically, and Eqs. (7)–(12) yield

$$\begin{aligned}&\eta f'''+f''+Reff''-Ref'^2\\ &-\beta_1 Re\Big(\frac{f^2f''}{\eta}+2f^2f'''-4ff'f''\Big)-MRe\Big(\frac{f'}{2}-\beta_1 ff''\Big)=0,\end{aligned} \tag{14}$$

$$2\eta^2 g'' + 2\eta g' - \frac{g}{2} + 2Re\eta f g' + Refg$$
$$- \beta_1 Re\Big(2f^2 g' + 4\eta f^2 g'' + 4ff'g - \frac{4f^2 g}{\eta}\Big) - MRe\Big(\eta g - 2\beta_1 \eta f g' - \beta_1 fg) = 0, \tag{15}$$

$$(1+R_{\rm d})(\eta\theta'' + \theta') + RePrf\theta' + PrN_{\rm b}\eta\theta'\phi' + PrN_{\rm t}\eta\theta'^2$$
$$+ Pr\delta Re\theta + PrReM(Ec_1 f'^2 + Ec_2 g^2) = 0 \quad \text{at} \quad \text{CWT}, \tag{16}$$

$$(1+R_{\rm d})(\eta\theta'' + \theta') + RePrf\theta' - PrRe\theta f' + PrN_{\rm b}\eta\theta'\phi'$$
$$+ PrN_{\rm t}\eta\theta'^2 + Pr\delta Re\theta + PrReM(Ec_1 f'^2 + Ec_2 g^2) = 0 \quad \text{at} \quad \text{PST}, \tag{17}$$

$$\eta\phi'' + \phi' + RePrLef\phi' + LePr\frac{N_{\rm t}}{N_{\rm b}}\theta' + LePr\frac{N_{\rm t}}{N_{\rm b}}\eta\theta'' = 0 \tag{18}$$

with the BCs

$$f(1) = 0, \quad f'(1) = 1, \quad g(1) = 1, \quad \theta'(1) = -\gamma_1(1 - \theta(1)), \quad \phi(1) = 1, \tag{19}$$
$$f'(\infty) = 0, \quad g(\infty) = 0, \quad \theta(\infty) = 0, \quad \phi(\infty) = 0. \tag{20}$$

In the above equations, $\beta_1 (= \lambda_1 a)$ is the Maxwell number, $Re\left(= \frac{aR_1^2}{2\nu}\right)$ is the Reynolds number, $M\left(= \frac{\sigma B_0^2}{\rho a}\right)$ is the magnetic number, $N_{\rm b}\left(= \frac{\tau D_{\rm B}\Delta C}{\nu}\right)$ is the Brownian motion parameter, $N_{\rm t}\left(= \frac{\tau D_{\rm T}\Delta T}{\nu T_\infty}\right)$ is the thermophoresis parameter, $R_{\rm d}\left(= \frac{16\sigma^* T_\infty^3}{3kk^*}\right)$ is the radiation parameter, $\delta\left(= \frac{Q_0}{\rho c_p a}\right)$ is the heat generation/absorption parameter, $Ec_1\left(= \frac{u_{\rm w}^2}{c_p\Delta T}\right)$ and $Ec_2\left(= \frac{v_{\rm w}^2}{c_p\Delta T}\right)$ are the Eckert numbers due to stretching and rotation of cylinder, respectively, $\gamma_1\left(= \frac{h_{\rm t}}{k}\sqrt{\frac{\nu}{a}}\right)$ is the Biot number, $Pr\left(= \frac{\nu}{\alpha_1}\right)$ is the Prandtl number, and $Le\left(= \frac{\alpha_1}{D_{\rm B}}\right)$ is the Lewis number.

In the study of viscous flow due to a stretching and rotating cylinder as reported by Fang and Yao[25], the solution convergence of the flow equations is too slow particularly for lower values of $Re$. Thus following Fang and Yao to make convergence fast, the variable $\eta$ is transformed as $\eta = \mathrm{e}^x$. Hence, Eqs. (14)–(20) become

$$f_{xxx} - 2f_{xx} + f_x - Re\left(f_x^2 - ff_{xx} + ff_x\right)$$
$$- \beta_1 Re\mathrm{e}^{-x}\left(2f^2 f_{xxx} - 5f^2 f_{xx} + 3f^2 f_x - 4ff_x f_{xx} + 4ff_x^2\right)$$
$$- MRe\Big(\mathrm{e}^x\frac{f_x}{2} - \beta_1 ff_{xx} + \beta_1 ff_x\Big) = 0, \tag{21}$$

$$2g_{xx} - \frac{g}{2} + Re(2fg_x + fg)$$
$$- \beta_1 Re\mathrm{e}^{-x}(2f^2 g_x + 4f^2 g_{xx} + 4f^2 g_x + 4ff_x g - 4f^2 g)$$
$$- MRe(\mathrm{e}^x g - 2\beta_1 fg_x - \beta_1 fg) = 0, \tag{22}$$

$$(1+R_{\rm d})\theta_{xx} + RePrf\theta_x + N_{\rm b}\theta_x\phi_x + N_{\rm t}\theta_x^2 + Pr\delta Re\mathrm{e}^x\theta$$
$$+ PrReM(Ec_1\mathrm{e}^{-x}f_x^2 + Ec_2\mathrm{e}^x g^2) = 0 \quad \text{at} \quad \text{CWT}, \tag{23}$$

$$(1+R_{\rm d})\theta_{xx} + RePrf\theta_x - PrRe\theta f_x + N_{\rm b}\theta_x\phi_x + N_{\rm t}\theta_x^2$$
$$+ Pr\delta Re\mathrm{e}^x\theta + PrReM(Ec_1\mathrm{e}^{-x}f_x^2 + Ec_2\mathrm{e}^x g^2) = 0 \quad \text{at} \quad \text{PST}, \tag{24}$$

$$\phi_{xx} + RePrLef\phi_x + LePr\frac{N_{\rm t}}{N_{\rm b}}\theta_{xx} = 0 \tag{25}$$

with the transformed BCs

$$f(0)=0,\quad f_x(0)=1,\quad g(0)=1,\quad \theta_x(0)=-\gamma_1(1-\theta(0)),\quad \phi(0)=1, \tag{26}$$

$$\lim_{x\to\infty} \mathrm{e}^{-x} f_x=0,\quad g(\infty)=0,\quad \theta(\infty)=0,\quad \phi(\infty)=0. \tag{27}$$

In the above equations, the subscript $x$ denotes the derivative with respect to $x$.

The Nusselt and Sherwood numbers $(Nu, Sh)$ are defined as

$$Nu=\frac{R_1 q_s}{k(T_\mathrm{w}-T_\infty)},\quad Sh=\frac{R_1 j_s}{D_\mathrm{B}(C_\mathrm{w}-C_\infty)}, \tag{28}$$

where $q_s$ and $j_s$ are the heat and mass fluxes, respectively, defined as

$$q_s=-k\Big(\frac{\partial T}{\partial r}\Big)_{r=R_1},\quad j_s=-D_\mathrm{B}\Big(\frac{\partial C}{\partial r}\Big)_{r=R_1}. \tag{29}$$

The dimensionless form of Eq. (28) is given by

$$Nu=-2\theta'(1),\quad Sh=-2\phi'(1). \tag{30}$$

## 3 Numerical solution

This section is proposed for the numerical solutions of established ODEs representing the flow and energy transport equations (21)–(25) along with BCs in Eqs. (26) and (27). The built-in MATLAB technique namely bvp4c is used to acquire the numerical results. The bvp4c is a finite difference technique that uses the three-stage Lobatto III formula. This is a collocation formula and the collocation polynomial provides a $C^1$-continuous solution with the fourth or accuracy on the given interval. The mesh and error control are strongly based on the residual of the solution. In order to use the bvp4c scheme, the governing ODEs are transformed into the system of the first-order ODEs by using the transformed variables as $f=y_1$, $f_x=y_2$, $f_{xx}=y_3$, $f_{xxx}=yy_1$, $g=y_4$, $g_x=y_5$, $g_{xx}=yy_2$, $\theta=y_6$, $\theta_x=y_7$, $\theta_{xx}=yy_3$, $\phi=y_8$, $\phi_x=y_9$, and $\phi_{xx}=yy_4$ for Eqs. (21)–(25). The resulting first-order ODEs are listed as follows:

$$\begin{aligned} yy_1=\Big(&2y_3-y_2+Re(y_2^2-y_1y_3+y_1y_2)\\ &+\beta_1 Re\mathrm{e}^{-x}(3y_1^2y_2-5y_1^2y_3-4y_1y_2y_3+4y_1y_2^2)\\ &+MRe\Big(\mathrm{e}^x\frac{y_2}{2}-\beta_1y_1y_3+\beta_1y_1y_2\Big)\Big)/a_1, \end{aligned} \tag{31}$$

$$\begin{aligned} yy_2=\Big(&\frac{y_4}{2}-2Rey_1y_5-Rey_1y_4+\beta_1Re\mathrm{e}^{-x}(6y_1^2y_5+4y_1^2y_2y_4-4y_1^2y_4)\\ &+MRe(\mathrm{e}^xy_4-2\beta_1y_1y_5-\beta_1y_1y_4)\Big)/a_2, \end{aligned} \tag{32}$$

$$\begin{aligned} yy_3=(&-RePry_1y_7-PrN_\mathrm{b}y_7y_9-PrN_\mathrm{t}y_7^2-Pr\delta Re\mathrm{e}^xy_6\\ &-PrReM(Ec_1\mathrm{e}^{-x}y_2^2+Ec_2\mathrm{e}^xy_4^2))/b_1\quad\text{at}\quad\text{CWT}, \end{aligned} \tag{33}$$

$$\begin{aligned} yy_3=(&-RePry_1y_7-PrN_\mathrm{b}y_7y_9-PrN_\mathrm{t}y_7^2-Pr\delta Re\mathrm{e}^xy_6\\ &+PrRey_2y_6-PrReM(Ec_1\mathrm{e}^{-x}y_2^2+Ec_2\mathrm{e}^xy_4^2))/b_1\quad\text{at}\quad\text{PST}, \end{aligned} \tag{34}$$

$$yy_4=-ReLePry_1y_9-LePr\frac{N_\mathrm{t}}{N_\mathrm{b}}yy_3, \tag{35}$$

where

$$a_1=1-2\beta_1Re\mathrm{e}^{-x}y_1^2,\quad a_2=2-4\beta_1Re\mathrm{e}^{-x}y_1^2,\quad b_1=1+R_\mathrm{d},$$

and the corresponding BCs are

$$y_1(0) = 0, \quad y_2(0) = 1, \quad y_4(0) = 1, \quad y_7(0) = -\gamma_1(1 - y_6(0)), \quad y_8(0) = 1, \tag{36}$$

$$\lim_{x\to\infty} \mathrm{e}^{-x} y_2 = 0, \quad y_4(\infty) = 0, \quad y_6(\infty) = 0, \quad y_8(\infty) = 1. \tag{37}$$

## 4 Discussion of results

The analysis of thermal energy transport in the swirling flow of Maxwell nanofluid with the effects of heat generation/absorption, thermal radiation, and resistive heating is the basic theme of our study. In this section of the study, we demonstrate the numerical results with physical description for flow and heat transport under the effect of the involved physical parameters, such as Reynolds number $Re$, Maxwell parameter $\beta_1$, magnetic parameter $M$, thermophoretic parameter $N_\mathrm{t}$, Brownian motion parameter $N_\mathrm{b}$, radiation parameter $R_\mathrm{d}$, Eckert numbers $(Ec_1, Ec_2)$, heat source/sink $\delta$, Biot number $\gamma_1$, Prandtl number $Pr$, and Lewis number $Le$. Throughout the numerical computation, we fix the values of pertinent parameters for thermal analysis as $Re = 3$, $M = 1$, $\beta_1 = N_\mathrm{t} = N_\mathrm{b} = \gamma_1 = R_\mathrm{d} = 0.5$, $Ec_1 = Ec_2 = \delta = 0.01$, and $Pr = Le = 6.5$. In case of flow analysis, we just change the values of $Pr = Le = 2.5$ for appropriate results. Figures 2(a)–2(c) show that for higher values of $Re$, the flow field declines and flow occurs only near the surface. Physically, the inertial force in the fluid flow increases due to higher values of $Re$. The inertial force is an opposing force for the fluid flow agent, which causes to decrease the flow field in all directions.

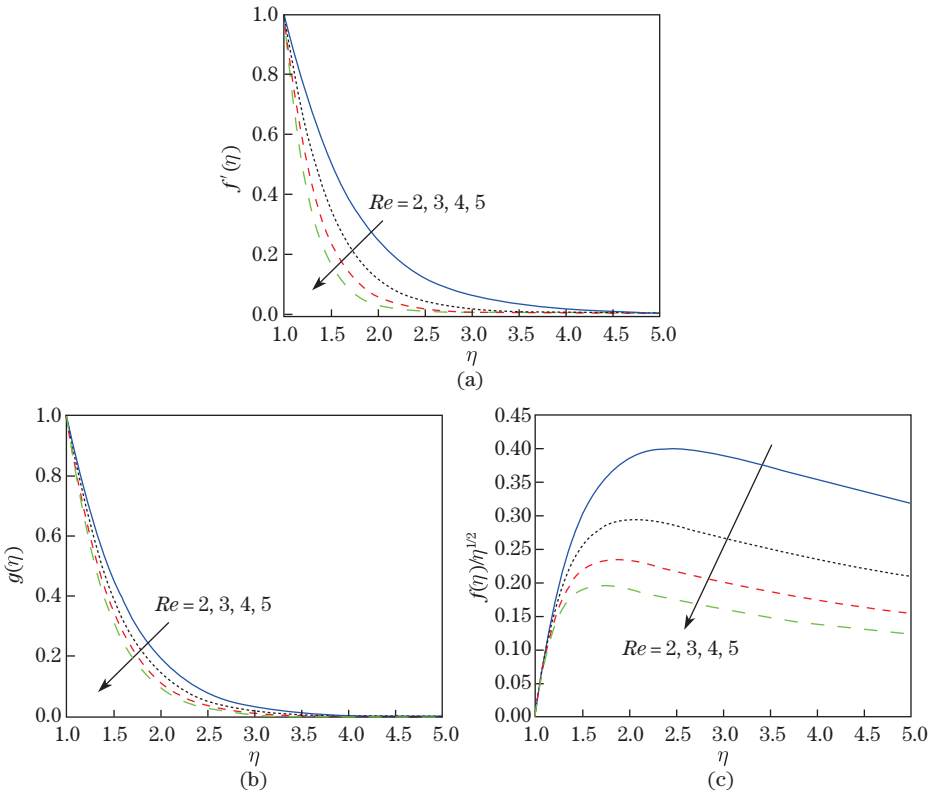


**Fig. 2** Axial, swirl, and radial velocity profiles via $Re$ (color online)

The impact of Maxwell parameter $\beta_1$ on the velocity field is deliberated in Figs. 3(a)–3(c). The higher values of $\beta_1$ boost up the stress relaxation phenomenon in viscoelastic fluid, and

consequently the decline in velocity field is observed. Moreover, it is noted that the impact of $\beta_1$ on axial component of velocity is prominent as compared with swirl component of velocity because of $\beta_1$, which is dimensionless with stretching rate of cylinder. The impacts of Reynolds number $Re$ and Maxwell number $\beta_1$ on temperature distribution are envisioned in Figs. 4(a) and 4(b). The results reveal that higher estimation in $Re$ decreases the temperature field, but the converse trend is found for $\beta_1$. Physically, due to the solid like response of viscoelastic material in case of higher stress relaxation phenomenon, the conduction of thermal energy enhances between the particles of the material, and as a result, the temperature distribution increases. We know that the higher value of $Re$ reduces the forced convection mechanism in the flow, which causes to decline the temperature field.

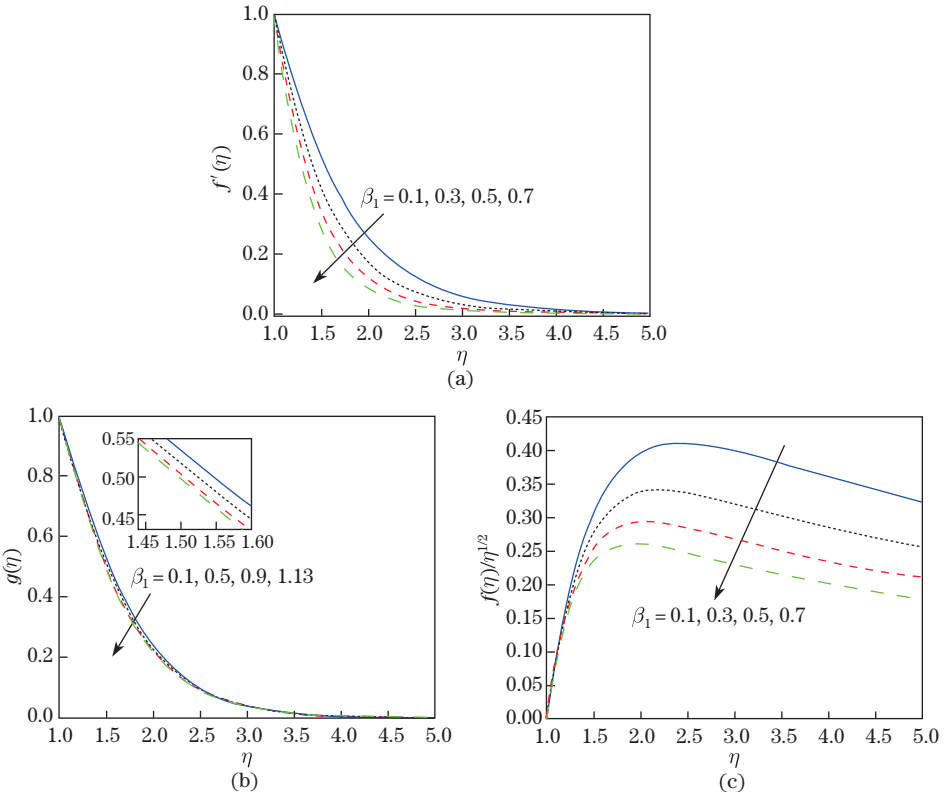


**Fig. 3** Axial, swirl, and radial velocity profiles via $\beta_1$ (color online)

The thermo-migration and haphazard motions of nano-size particles in flow of Maxwell fluid are described by the dimensionless parameters $N_{\rm t}$ and $N_{\rm b}$. The heat transport in the flow is significantly enhanced with higher values of thermophoretic and Brownian motion paramters $N_{\rm t}$ and $N_{\rm b}$. Physically, higher values of thermophoretic parameter $N_{\rm t}$ enhance the thermal gradient in fluid particles, which results in the enhancement of heat transport. Furthermore, due to the increasing trend of Brownian diffusion parameter $N_{\rm b}$, the particle collisions and nanoconvection are enhanced. Therefore, the thermal energy transport increases. These results are explored in Figs. 5(a) and 5(b).

The heat source $\delta$ ($> 0$) in the system produces extra heat which increases the heat transport in the fluid flow and the converse is true for the heat sink $\delta < 0$. The results for $\delta > 0$ and $\delta < 0$ are presented in Figs. 6(a) and 6(b). Figures 7(a) and 7(b) depict the effect of Eckert numbers $Ec_1$ and $Ec_2$ on temperature distribution in the Maxwell fluid flow. It is observed that there

is higher transport in the thermal energy due to augmentation in $Ec_1$ and $Ec_2$. Physically, the Eckert number describes the Joule heating effect in the system which is the ratio of kinetic energy of the flow to the thermal energy transport driving force. Higher values of $Ec_1$ and $Ec_2$ increase the temperature field because the advection mechanism for heat transport in the flow enhances and heat dissipation reduces. Moreover, it is noted that the effect of $Ec_2$ is more prominent on the temperature field as compared with $Ec_1$.

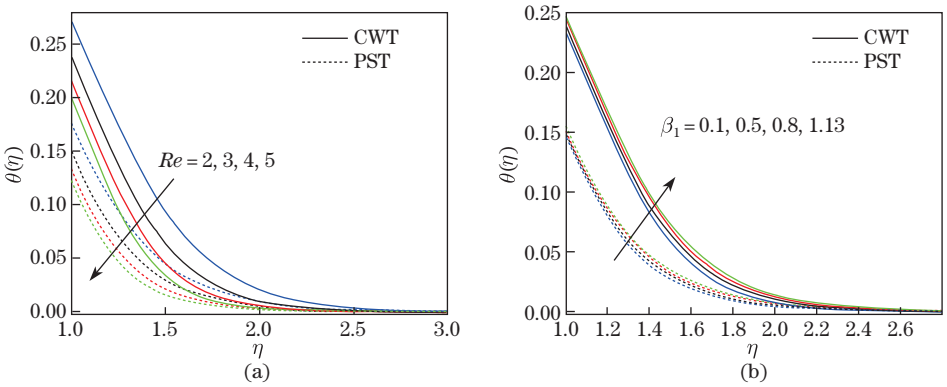


**Fig. 4** Temperature profiles via $Re$ and $\beta_1$ (color online)

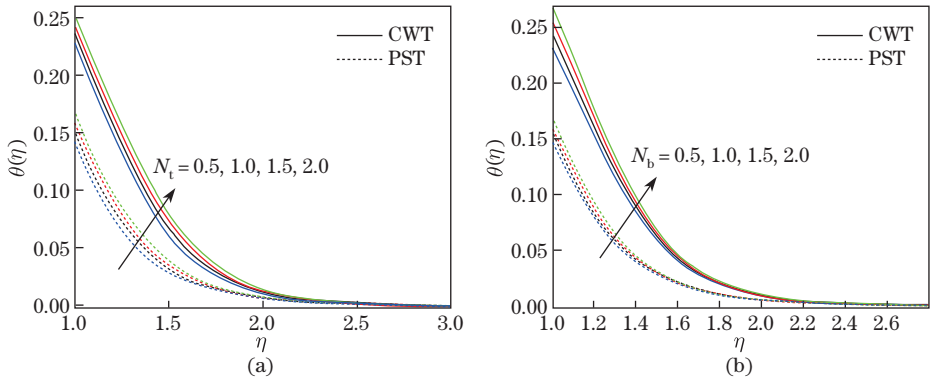


**Fig. 5** Temperature profiles via $N_t$ and $N_b$ (color online)

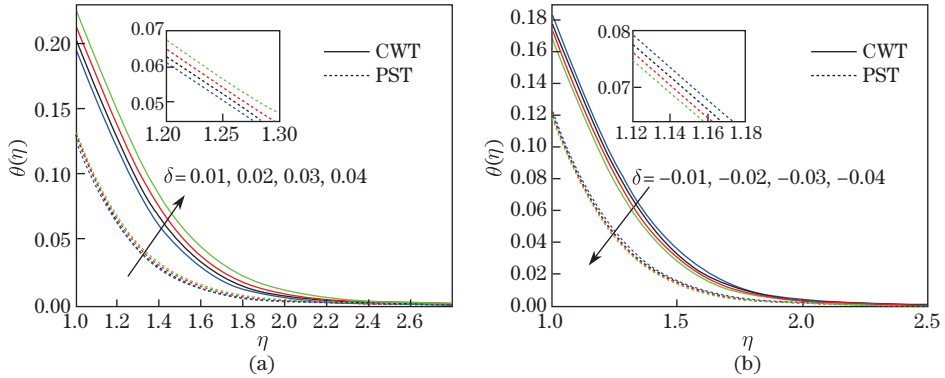


**Fig. 6** Temperature profiles via $\delta$ (color online)

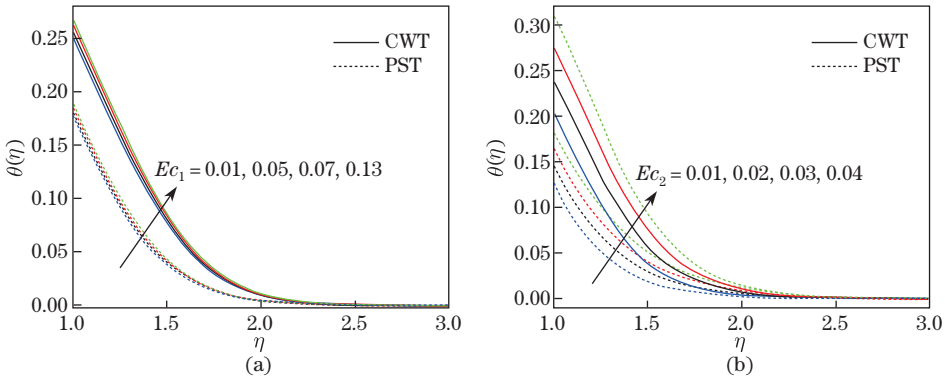


**Fig. 7** Temperature profiles via $Ec_1$ and $Ec_2$ (color online)

Figures 8(a) and 8(b) show that both the radiative parameter $R_{\mathrm{d}}$ and Biot number $\gamma_1$ boost up the temperature field. Physically, the Biot number increases thermal gradient at the surface of cylinder due to decrease in the resistance for energy transport inside to outside of the body. In view of this physical justification, the temperature field enhances. The thermal energy transport in the fluid flow is a decreasing function of Prandtl number $Pr$ for higher values as given in Fig. 9.

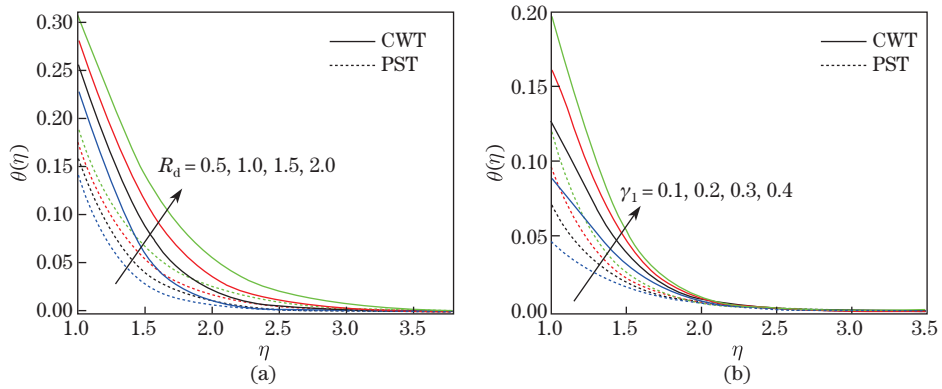


**Fig. 8** Temperature profiles via $R_{\mathrm{d}}$ and $\gamma_1$ (color online)

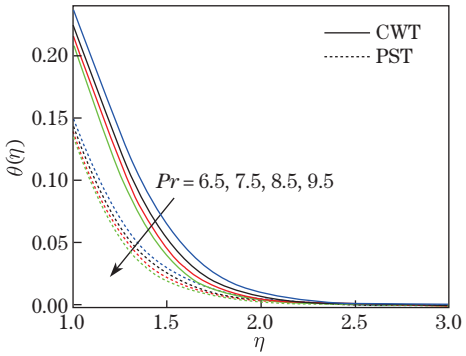


**Fig. 9** Temperature profile via $Pr$ (color online)

In the whole thermal analysis, we conclude that there is higher transport of thermal energy in fluid flow for CWT as compared with PST. Physically in case of PST, the axial varying temperature of surface of cylinder declines the heat transport in the Maxwell fluid flow.

The outcomes acquired through numerical computation are validated through Table 1. The numerical values of thermal gradient against various pertinent parameters at the surface of cylinder for both surface heating agents CWT and PST are shown in Table 2. It is observed that there is a higher value of thermal gradient in case PST than CWT. Moreover, $Ec_2$ has more effects on the thermal gradient at the surface as compared with $Ec_1$.

**Table 1** Comparison values of axial $f''(1)$ and swirl $g'(1)$ velocity gradients for various $Re$ in the limiting case when $\beta_1 = M = 0$

| $Re$ | $f''(1)$ Ref. [25] | $g'(1)$ Ref. [25] | $f''(1)$ Present result | $g'(1)$ Present result |
|---|---|---|---|---|
| 0.1 | −0.481 80 | −0.510 19 | −0.488 907 | −0.501 542 |
| 0.2 | −0.617 48 | −0.526 05 | −0.610 423 | −0.528 809 |
| 0.3 | | | −0.711 562 | −0.563 363 |
| 0.4 | | | −0.797 618 | −0.585 919 |
| 0.5 | −0.882 20 | −0.584 88 | −0.809 541 | −0.608 461 |
| 1 | −1.177 75 | −0.687 72 | −1.177 669 | −0.697 671 |
| 2 | −1.593 89 | −0.872 63 | −1.596 640 | −0.869 605 |
| 3 | | | −1.911 086 | −1.038 214 |
| 4 | | | −2.178 536 | −1.178 690 |
| 5 | −2.417 43 | −1.297 88 | −2.417 865 | −1.297 590 |
| 10 | −3.344 46 | −1.810 06 | −3.340 094 | −1.800 194 |

**Table 2** Numerical values of the thermal gradient $\theta'(1)$ at the surface of the cylinder for different values of $Re$, $R_\mathrm{d}$, $\gamma_1$, $Ec_1$, $Ec_2$, $N_\mathrm{t}$, and $N_\mathrm{b}$ with fixed $\beta_1 = 0.5$, $M = 1$, and $Pr = Le = 6.5$

| $Re$ | $R_\mathrm{d}$ | $\gamma_1$ | $Ec_1$ | $Ec_2$ | $N_\mathrm{t}$ | $N_\mathrm{b}$ | $-\theta'(1)$(CWT) | $-\theta'(1)$(PST) |
|---|---|---|---|---|---|---|---|---|
| 1 | 0.5 | 0.5 | 0.01 | 0.01 | 0.5 | 0.5 | 0.333 702 1 | 0.373 227 6 |
| 2 | | | | | | | 0.360 540 6 | 0.398 206 5 |
| 3 | | | | | | | 0.374 073 2 | 0.410 892 3 |
| 3 | 0.5 | 0.5 | 0.01 | 0.01 | 0.5 | 0.5 | 0.374 406 3 | 0.410 892 3 |
| | 1.0 | | | | | | 0.364 650 4 | 0.405 150 5 |
| | 1.5 | | | | | | 0.355 844 9 | 0.399 725 9 |
| 3 | 0.5 | 0.5 | 0.01 | 0.01 | 0.5 | 0.5 | 0.374 106 1 | 0.410 892 3 |
| | | 1.0 | | | | | 0.580 786 0 | 0.673 408 5 |
| | | 1.5 | | | | | 0.700 781 7 | 0.842 118 8 |
| 3 | 0.5 | 0.5 | 0.01 | 0.01 | 0.5 | 0.5 | 0.374 106 1 | 0.410 892 3 |
| | | | 0.05 | | | | 0.371 370 0 | 0.409 061 7 |
| | | | 0.09 | | | | 0.368 648 7 | 0.407 239 2 |
| 3 | 0.5 | 0.5 | 0.1 | 0.01 | 0.1 | 0.5 | 0.374 106 1 | 0.410 892 3 |
| | | | | 0.03 | | | 0.353 913 6 | 0.398 837 6 |
| | | | | 0.05 | | | 0.333 869 7 | 0.386 841 1 |
| 3 | 0.5 | 0.5 | 0.1 | 0.1 | 0.5 | 0.5 | 0.374 106 1 | 0.387 962 5 |
| | | | | | 1.0 | | 0.356 610 6 | 0.376 908 7 |
| | | | | | 1.5 | | 0.340 123 8 | 0.366 697 1 |
| 3 | 0.5 | 0.5 | 0.1 | 0.1 | 0.1 | 0.5 | 0.374 106 1 | 0.387 962 5 |
| | | | | | | 1.0 | 0.371 347 3 | 0.384 962 3 |
| 1 | 0.5 | 0.5 | 0.01 | 0.01 | 0.5 | 1.5 | 0.368 562 2 | 0.381 910 3 |

## 5 Key points

The heat transport mechanism in the MHD swirling flow of Maxwell nanofluid induced by the stretching and rotating cylinder under the impact of Joule heating, thermal radiation, and heat source/sink is studied. The temperature of the surface of the cylinder is assumed as a constant and axially varying. The whole theoretical analysis is summarized through the following conclusions.

(I) The augmented temperature profile is observed in case of CWT as compared with PST.

(II) Higher values of the Reynolds number decrease both flow field and thermal energy distribution as well as reduce the penetration depth.

(III) Thermal and concentration distributions boost up while the flow field declines for higher values of the Maxwell parameter.

(IV) The impact of the Maxwell parameter is prominent on the axial velocity as compared with the swirl velocity.

(V) Increase in the temperature field is noted for a higher rate of thermo-migration and haphazard motion of nanoparticles in fluid flow.

(VI) The advective transport of thermal energy is enhanced for higher values of the Eckert number.

## References

[1] NACCACHE, M. F. and MENDES, P. R. S. Heat transfer to non-Newtonian fluids in laminar flow through rectangular ducts. *International Journal of Heat and Fluid Flow*, **17**, 613–620 (1996)

[2] SHIN, S. The effect of the shear rate-dependent thermal conductivity of non-Newtonian fluids on the heat transfer in a pipe flow. *International Communications in Heat and Mass Transfer*, **23**, 665–678 (1996)

[3] NOURI, J. M. and WHITELAW, J. H. Flow of Newtonian and non-Newtonian fluids in an eccentric annulus with rotation of the inner cylinder. *International Journal of Heat and Fluid Flow*, **18**, 236–246 (1997)

[4] ATTIA, H. A. Numerical study of flow and heat transfer of a non-Newtonian fluid on a rotating porous disk. *Applied Mathematics and Computation*. **163**, 327–342 (2005)

[5] DHINAKARAN, S., AFONSO, A. M., ALVES, M. A., and PINHO, F. T. Steady viscoelastic fluid flow between parallel plates under electro-osmotic forces: Phan-Thien-Tanner model. *Journal of Colloid and Interface Science*, **344**, 513–520 (2010)

[6] PRASAD, K. V., PAL, D., UMESH, V., and RAO, N. S. P. The effect of variable viscosity on MHD viscoelastic fluid flow and heat transfer over a stretching sheet. *Communications in Nonlinear Science and Numerical Simulation*, **15**, 331–344 (2010)

[7] MALASPINAS, O., FIÉTIER, N., and DEVILLE, M. Lattice Boltzmann method for the simulation of viscoelastic fluid flows. *Journal of Non-Newtonian Fluid Mechanics*, **165**, 1637–1653 (2010)

[8] SIDDIQA, S., BEGUM, N., HOSSAIN, M. D. A., and GORLA, R. S. R. Natural convection flow of a two-phase dusty non-Newtonian fluid along a vertical surface. *International Journal of Heat and Mass Transfer*, **113**, 482–489 (2017)

[9] MAHAPATRA, T. R. and SIDUI, S. Non-axisymmetric Homann stagnation-point flow of a viscoelastic fluid towards a fixed plate. *European Journal of Mechanics-B/Fluids*, **79**, 38–43 (2020)

[10] TAN, W. C., PAN, W. X., and XU, M. Y. A note on unsteady flows of a viscoelastic fluid with the fractional Maxwell model between two parallel plates. *International Journal of Non-Linear Mechanics*, **38**(5), 645–650 (2003)

[11] NADEEM, S., HAQ, R. U., and KHAN, Z. H. Numerical study of MHD boundary layer flow of a Maxwell fluid past a stretching sheet in the presence of nanoparticles. *Journal of the Taiwan Institute of Chemical Engineers*, **45**(1), 121–126 (2014)

[12] ABBASBANDY, S., NAZ, R., HAYAT, T., and ALSAEDI, A. Numerical and analytical solutions for Falkner-Skan flow of MHD Maxwell fluid. *Applied Mathematics and Computation*, **242**, 569–575 (2014)

[13] AHMED, J., KHAN, M., and AHMAD, L. MHD swirling flow and heat transfer in Maxwell fluid driven by two coaxially rotating disks with variable thermal conductivity. *Chinese Journal of Physics*, **60**, 22–34 (2019)

[14] RAUF, A., MAHSUD, Y., and SIDDIQUE, I. Multi-layer flows of immiscible fractional Maxwell fluids in a cylindrical domain. *Chinese Journal of Physics* (2019) https://doi.org/10.1016/j.cjph.2019.09.015

[15] KUMARI, M. and NATH, G. Analytical solution of unsteady three-dimensional MHD boundary layer flow and heat transfer due to impulsively stretched plane surface. *Communications in Nonlinear Science and Numerical Simulation*, **14**, 3339–3350 (2009)

[16] ASHORYNEJAD, H. R., SHEIKHOLESLAMI, M., POP, I., and GANJI, D. D. Nanofluid flow and heat transfer due to a stretching cylinder in the presence of magnetic field. *Heat and Mass Transfer*, **49**(3), 427–436 (2013)

[17] TURKYILMAZOGLU, M. MHD fluid flow and heat transfer due to a shrinking rotating disk. *Computers & Fluids*, **90**, 51–56 (2014)

[18] SAHOO, B. and SHEVCHUK, I. V. Heat transfer due to revolving flow of Reiner-Rivlin fluid over a stretchable surface. *Thermal Science and Engineering Progress*, **10**, 327–336 (2019)

[19] KHAN, M., AHMED, J., and AHMAD, L. Chemically reactive and radiative von Kármán swirling flow due to a rotating disk. *Applied Mathematics and Mechanics* (*English Edition*), **39**(9), 1295–1310 (2018) https://doi.org/10.1007/s10483-018-2368-9

[20] TURKYILMAZOGLU, M. Analytical solutions to mixed convection MHD fluid flow induced by a nonlinearly deforming permeable surface. *Communications in Nonlinear Science and Numerical Simulation*, **63**, 373–379 (2018)

[21] AHMED, J., KHAN, M., and AHMAD, L. Stagnation point flow of Maxwell nanofluid over a permeable rotating disk with heat source/sink. *Journal of Molecular Liquids*, **287**, 110853 (2019)

[22] MEHMOOD, A., USMAN, M., and WEIGAND, B. Heat and mass transfer phenomena due to a rotating non-isothermal wavy disk. *International Journal of Heat and Mass Transfer*, **129**, 96–102 (2019)

[23] THAKUR, P., TIWARI, N., and CHHABRA, R. P. Momentum and heat transfer from an asymmetrically confined rotating cylinder in a power-law fluid. *International Journal of Thermal Sciences*, **137**, 410–430 (2019)

[24] RAJAGOPAL, K. R. A note on novel generalizations of the Maxwell fluid model. *International Journal of Non-Linear Mechanics*, **47**(1), 72–76 (2012)

[25] FANG, T. and YAO, S. Viscous swirling flow over a stretching cylinder. *Chinese Physics Letters*, **28**, 114702 (2011)